International Journal of Biological Macromolecules 308 (2025) 142254

Contents lists available at ScienceDirect

International Journal of Biological Macromolecules

journal homepage: www.elsevier.com/locate/ijbiomac

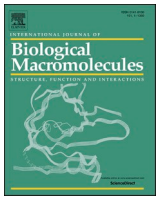

Longan-inspired chitosan-pectin core-shell hydrogel beads for oral delivery of biodrugs to enhance osteoporosis therapy

V.H. Giang Phan [a,1], Bich-Phuong Thi Nguyen [a,1], Nhi Yen Nguyen [a], Cam-Nhung Dinh Tran [a], Quynh-Nhu Doan Nguyen [a], Cuong Hung Luu [b,c], Panchanathan Manivasagan [d], Eue-Soon Jang [d], Deok Chun Yang [e], Dong Uk Yang [f,*], Yi Li [g,*], João Conde [h,*], Thavasyappan Thambi [e,*]

[a] Biomaterials and Nanotechnology Research Group, Faculty of Applied Sciences, Ton Duc Thang University, Ho Chi Minh City, Vietnam
[b] School of Environment and Science, Griffith University, Nathan, QLD 4111, Australia
[c] Queensland Micro- and Nanotechnology Centre, Griffith University, Nathan, QLD 4111, Australia
[d] Department of Applied Chemistry, Kumoh National Institute of Technology, Daehak-ro 61, Gumi, Gyeongbuk 39177, Republic of Korea
[e] Graduate School of Biotechnology, College of Life Sciences, Kyung Hee University, Yongin si, Gyeonggi do 17104, Republic of Korea
[f] AIBIOME, 6, Jeonmin-ro 30beon-gil, Yuseong-gu, Daejeon 34214, Republic of Korea
[g] College of Materials and Textile Engineering & Nanotechnology Research Institute, Jiaxing University, Jiaxing 314001, Zhejiang Province, PR China
[h] Comprehensive Health Research Centre (CHRC), NOVA Medical School, Faculdade de Ciências Médicas, NMS|FCM, Universidade Nova de Lisboa, Lisboa, Portugal

ARTICLE INFO

Keywords:
Pectin
Chitosan
MSNs
Oral drug delivery
Intestine-targeted drug delivery
Osteoporosis

ABSTRACT

Osteoporosis, a common disorder, is characterized by a systemic reduction in bone mass and structural integrity, resulting in brittle bones. Reducing bone loss and enhancing bone density through oral administration of biopharmaceuticals provides significant advantages, including convenience and non-invasiveness for patients. However, challenges such as poor absorption and enzymatic degradation necessitate the development of innovative drug delivery systems. This research introduces a core-shell hydrogel system inspired by the natural architecture of Longan fruit, constructed from pectin and chitosan biopolymers, designed to create biocapsules and sustain the release of biodrugs. In this system, salmon calcitonin (sCT) was encapsulated within mesoporous silica nanoparticles (MSNs) and incorporated into the core of the beads. The synthesis of the core-shell hydrogel beads was carefully regulated by adjusting the immersion time and concentration of the crosslinker. The hydrogel beads demonstrated durability, with the pectin shell effectively preventing rapid degradation in the stomach, while the chitosan layer enhanced adhesion to the intestinal walls, safeguarded sCT, and enabled sustained drug release over an extended period of up to 30 h. Furthermore, biocompatibility tests indicated minimal cytotoxicity and hemolysis. Cellular uptake assays demonstrated that the core-shell beads effectively encapsulated sCT and ensured its prolonged release to CT-26 cells. This study presents a promising platform for oral sCT delivery, offering enhanced efficacy, patient compliance, and a potential replacement for injection-based therapies.

1. Introduction

In recent decades, considerable efforts have been invested in exploring alternatives to injection for the administration of macromolecules, particularly peptides and proteins [1]. Notably, transmucosal routes, such as the nasal, pulmonary, and oral routes, have garnered significant attention [2–4]. However, the oral administration of large macromolecules requires further investigation. Challenges arise from the harsh conditions of the gastrointestinal tract (GIT) and the limited permeability of the intestinal barrier, making solutions elusive [5]. Moreover, protein and peptide-based drugs are susceptible to hydrolysis and breakdown by proteolytic enzymes [6,7]. Despite these obstacles,

* Corresponding authors.
E-mail addresses: phanvuhoanggiang@tdtu.edu.vn (V.H.G. Phan), rudckfeo23@naver.com (D.U. Yang), liyi@zjxu.edu.cn (Y. Li), joao.conde@nms.unl.pt (J. Conde), thambi@khu.ac.kr (T. Thambi).
[1] These authors contributed equally.

https://doi.org/10.1016/j.ijbiomac.2025.142254
Received 15 November 2024; Received in revised form 12 March 2025; Accepted 16 March 2025
Available online 20 March 2025

oral medications offer the benefits of convenience, non-invasiveness, precise targeting of diseased tissues, controlled release rates, improved adherence, and patient comfort [8]. Consequently, the oral route is considered the most optimal method due to its ease of control, user-friendliness, and advantages for patients [9].

The incidence of osteoporosis is increasing, and the primary objective of its treatment is to prevent bone fractures by minimizing bone loss or, ideally, enhancing bone density and strength [10]. Calcitonin is a common therapeutic agent for various bone-related conditions, including hypercalcemia, Paget's disease, and osteoporosis [11–13]. In the context of osteoporosis, calcitonin plays a crucial role in reducing bone resorption and alleviating bone pain, a prevalent symptom associated with this condition [14]. In clinical practice, synthetic or recombinant salmon calcitonin (sCT) is widely used [15]. This is attributed to its 50 % sequence homology with human calcitonin, coupled with a remarkable 40–50 times higher potency than human calcitonin, owing to its increased affinity toward the human calcitonin receptor [16]. Salmon calcitonin is commonly administered *via* intramuscular or subcutaneous injection and is also available as a nasal spray [17]. However, discomfort and reduced patient compliance associated with frequent administration pose challenges, leading to poor adherence and treatment gaps. Additionally, intranasal calcitonin administration has been linked to an increased incidence of nosebleeds, runny nose, and other nasal irritations. Although oral formulations have been extensively investigated, they exhibit low bioavailability owing to enzymatic degradation in the digestive tract and poor intestinal absorption [18].

To address the challenges associated with peptide therapeutics, extensive research and development efforts have focused on various drug carrier systems, with hydrogels standing out because of their considerable potential for drug delivery and diverse biomedical applications, such as tissue engineering. The physiology of the gastrointestinal (GI) tract is highly complex, characterized by abrupt pH changes along its length [19,20]. These variations include an acidic pH in the stomach, slightly acidic to neutral conditions in the small intestine, and mildly basic conditions in the large intestine [21]. These distinctive characteristics pose challenges for formulation scientists aiming to target medicines to specific locations within the intestine through oral administration. This challenge is particularly pronounced when drugs are prematurely released in the stomach, leading to a loss of therapeutic efficacy because of the inability to reach the intended site [22,23]. Developing formulations that can navigate these dynamic environments and effectively deliver drugs to specific GI locations is crucial for optimizing oral drug delivery.

The innovation of core-shell structures in drug delivery, particularly for oral administration, has introduced significant advancements in overcoming the challenges posed by the gastrointestinal environment [24]. Core-shell structured carriers provide superior advantages compared to conventional structures. The shell protects the integrity of the system in the stomach. When the system passes through the stomach, the shell gradually swells or degrades, triggering the release of the payload in the core at the intestinal site. In summary, core-shell structures shield therapeutic agents from harsh gastric conditions and ensure controlled release and improved bioavailability [25,26].

In this study, chitosan and pectin were selected as key components because of their complementary properties and suitability for oral drug delivery systems. Chitosan, a cationic biopolymer derived from chitin comprising *N*-acetyl glucosamine and glucosamine, offers unique characteristics such as biocompatibility, biodegradability, and high modification flexibility, making it an ideal candidate for biomedical applications and drug delivery [27]. Owing to the presence of amino groups along the chain backbone, chitosan molecules can interact electrostatically with the negatively charged groups of the mucus layer. This mucoadhesive ability enhances the adherence of chitosan-based carriers to the intestinal region, thereby improving drug retention and absorption [28]. Additionally, chitosan possesses pH-responsive properties, particularly in terms of pH-dependent swelling behavior and solubility, enabling it to modulate drug release at specific pH values. Pectin, an anionic polysaccharide extracted from plant cell walls, consists of 1,4-linked D-galacturonic acid units. One of the most interesting properties of pectin is its calcium-dependent gelation ability, in which strong physical cross-links are formed through the binding between Ca^{2+} ions and COO^- groups in pectin, frequently described by the "egg-box" model. Pectin-based hydrogels exhibit high stability, mechanical strength, non-toxicity, and excellent water-holding capacities. Similar to chitosan, pectin is an ideal material for developing drug delivery systems and tissue engineering scaffolds [29]. Moreover, pectin demonstrates inherent resistance to acidic environments, proteases, and amylases in the upper gastrointestinal tract. In the low pH environment of the stomach, the carboxyl groups within pectin molecules become protonated, causing the pectin layer to shrink and become more compact, offering excellent drug protection for oral delivery systems [30]. Therefore, pectin can act as a temporary protective shell for the chitosan core, ensuring that the system remains intact during transit through the stomach [31].

To further enhance the drug-loading efficiency, mesoporous silica nanoparticles (MSNs) were integrated into the system. With their high surface area, tunable pore size, and dense negative surface charges, MSNs act as intermediaries between sCT and the positively charged chitosan core [32,33]. This design not only increases the drug loading capacity but also optimizes the use of natural materials, resulting in a robust and environmentally sustainable delivery platform.

In this study, core-shell-structured hydrogel beads were developed using chitosan and pectin in combination with MSNs to enhance the efficiency of sCT oral drug delivery for osteoporosis treatment, as illustrated in Fig. 1. Biocapsules were synthesized directly from these materials using a straightforward dropwise method, with careful control over the key factors influencing the characterization of the core-shell hydrogel beads. Additionally, the integration of MSNs was evaluated for its contribution to improving drug loading capacity and modulating sCT-release efficiency. The biocompatibility of the system was assessed using cellular and chorioallantoic membrane (CAM) assays. This design offers superior protection for sCT against the harsh conditions of the gastrointestinal tract, demonstrating its potential as an advanced platform for oral peptide drug delivery with improved therapeutic efficacy.

2. Materials and methods

2.1. Materials

Iron(II) chloride tetrahydrate ($FeCl_2{\cdot}4H_2O$, 98 %), iron(III) chloride hexahydrate ($FeCl_3{\cdot}6H_2O$, 98 %, ammonium hydroxide (NH_4OH, 28–30 % NH_3), cetyltrimethylammonium bromide (CTAB, $\geq$ 98 %), tetraethyl orthosilicate (TEOS, $\geq$ 98 %), pectin (from citrus peel, galacturonic acid $\geq$74.0 %), chitosan (75–85 % deacetylated, 190–375 kDa) were obtained from Sigma-Aldrich (MO, USA). Calcium chloride ($CaCl_2$, 96 %) was purchased from Merck (Darmstadt, Germany). Salmon calcitonin (sCT) was acquired from the Novartis Site (Stein, Switzerland). Analytical grade solvents were sourced from Thermo Fisher Scientific (MA, USA). All chemicals were used without further purification.

2.2. Characterization methods

2.2.1. Morphology

Scanning electron microscope (SEM, JSM-6510, JEOL Ltd., Japan) and transmission electron microscope (TEM, JEM-2100, JEOL Ltd., Japan) were employed to examine the morphology and size distribution of nanoparticles.

2.2.2. Infrared spectroscopy

Fourier-transform infrared spectrophotometer (FTIR, Spectrum Two FT-IR, PerkinElmer, USA) was used to assess the chemical composition.

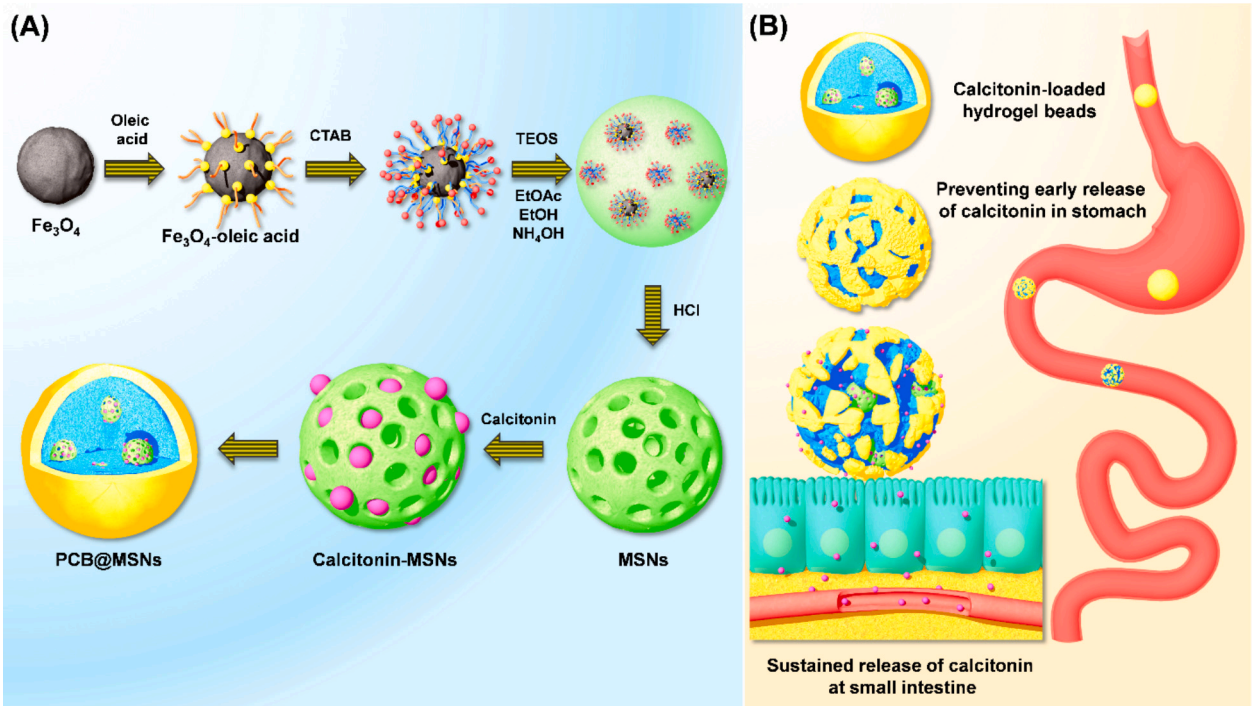

Fig. 1. Schematic representation of the structural design of PCB@MSNs for small intestine-targeted calcitonin delivery in the treatment of osteoporosis. (A) Schematic illustration of the synthesis of PCB@MSNs inspired by the natural architecture of the longan fruit. Uniformly porous silica nanoparticles (MSNs) were synthesized using iron oxide-oleic acid and cetyltrimethylammonium bromide (CTAB) templates. Subsequently, calcitonin (sCT) was loaded into the MSNs, which were sequentially covered with chitosan and pectin to generate core-shell beads, PCB@MSNs. (B) Oral administration of PCB@MSNs successfully passed through the harsh acidic environment of the stomach, effectively preventing the premature release of sCT. After the delivery of PCB@MSNs to the small intestine, the slow bead swelling and degradation led to sustained sCT release, enhancing its penetration.

2.2.3. Crystallography

X-ray powder diffraction (XRD) patterns were recorded using a PW1820/1710 diffractometer (Phillips, Netherlands) with Bragg-Brentano geometry (Cu K_α, $\lambda = 1.5406$ Å) to analyze the structure of MSNs and hydrogel beads.

2.2.4. Surface area analysis

Specific area was evaluated based on Brunner-Emmett-Teller (BET) theory using Nova 600 BET instrument (Quantachrome Instruments, USA).

2.3. Synthesis of iron oxide nanoparticles (Fe_3O_4 NPs)

The co-precipitation method was employed for the synthesis of Fe_3O_4 NPs. To initiate the process, 6 mL of $FeCl_2{\cdot}4H_2O$ (0.75 mol·L^{-1}) and 7.5 mL of $FeCl_3{\cdot}6H_2O$ (1 mol·L^{-1}) were dissolved in 300 mL of distilled water under vigorous stirring at room temperature. Subsequently, ammonia solution was gradually added using a syringe to maintain a reaction pH of 10. A rapid color change from dark yellow to black was observed, indicating the formation of Fe_3O_4 NPs. To enhance the dispersion stability of the nanoparticles, 1.5 g of oleic acid (OA), acting as a surfactant, was introduced into the reaction system. The resulting Fe_3O_4 NPs were isolated *via* magnetic decantation and further purified by washing with ethanol. Finally, the Fe_3O_4 nanoparticles were dried at 60 °C for 1 h.

2.4. MSNs synthesis

MSNs were prepared as described previously, with minor modifications [34]. Initially, a solution of CTAB (0.1 g) in 10 mL distilled water was prepared. Subsequently, 0.5 mL OA stabilized Fe_3O_4 NPs in chloroform (6.0 mg·mL^{-1}) were vigorously stirred with the CTAB solution for 20 min in a round-bottom flask. The mixture was heated to 60 °C for 30 min to remove the chloroform. In a separate flask, a solution comprising 5 mL methanol, 20 mL ethyl acetate, 3 mL NH_4OH, and 100 mL distilled water was prepared. The two resulting solutions were combined and continuously stirred, and 0.5 mL of TEOS was added to the reaction mixture. The sol-gel reaction proceeded at 60 °C for 8 h to allow for the formation of nanoparticles. The nanoparticles were then isolated and washed four times with absolute ethanol. To remove the structural framework, the silica nanoparticles were vigorously agitated in 20 mL of 10 % ethanolic HCl for 3 h at 60 °C, yielding in a crude mixture of MSNs. This mixture was washed three times with ethanol and subsequently dried at 60 °C for 3 h to obtain a white MSN powder.

2.5. Preparation of pectin-chitosan core-shell beads and effect of $CaCl_2$ concentration on properties of PCBs

A chitosan solution with a concentration of 4.5 % w/v was prepared by dissolving 1.35 g of chitosan in 30 mL of 1 % glacial acetic acid solution. The mixture was stirred for approximately 30 min to ensure complete dissolution of the chitosan. Following this, varying concentrations of $CaCl_2$ (0.25 mol·L^{-1}, 0.50 mol·L^{-1}, and 1 mol·L^{-1}) were added, and the solutions were stirred continuously for 2 h, resulting in $CaCl_2$-containing chitosan solutions. Simultaneously, a 3 % w/v pectin solution was prepared, with its pH adjusted to 9 using 1 mol·L^{-1} NaOH. The $CaCl_2$-chitosan solutions were then loaded into syringes and carefully dripped into a beaker containing the pectin solution from a fixed height of 5 cm. Gentle stirring was performed to prevent the hydrogel beads from clumping together. The beads were further incubated in the pectin solution for 5–45 min to solidify their structures. The beads were then collected and thoroughly washed with distilled water. For long-term preservation, the samples were frozen and freeze-dried. The resulting beads were designated as PCB_1, PCB_2, and PCB_3, with increasing $CaCl_2$ concentrations. Chitosan beads (labeled as CB) were separately prepared by directly dripping the chitosan solution into a pH

9 PBS solution.

2.6. Preparation of MSNs embedded PCB

PCB_2 was employed as the base for embedding MSNs into the bead core. A 4.5 % w/v chitosan solution was prepared, to which $CaCl_2$ (0.5 $mol{\cdot}L^{-1}$) and MSNs (5 mg/mL) were added. The mixture was stirred thoroughly to ensure homogeneity. The resulting solution was loaded into a syringe and dripped into a 3 % w/v pectin solution (pH 9) to synthesize PCB@MSNs. For the preparation of sCT-loaded PCB@MSNs, sCT was pre-mixed with MSNs in PBS at a 2:5 (w/w) ratio before undergoing the same bead fabrication process. After synthesis, the beads were washed with deionized water, freeze-dried and stored at 4 °C to maintain stability until use.

2.7. Swelling behavior of hydrogel beads in GIT fluids

Investigating the swelling capacity of hydrogel beads under varying pH conditions provides crucial insights into their ability to retain and stabilize drugs within the diverse environments of the digestive system. To investigate this behavior, freeze-dried hydrogel beads were immersed in simulated gastric fluid (SGF, pH 1.2), simulated intestinal fluid (SIF, pH 6.8), and simulated colonic fluid (SCF, pH 7.4). At predetermined time intervals, the beads were retrieved, and excess water was gently blotted using absorbent paper. The weights of the hydrated beads were then recorded to calculate the swelling ratio. The swelling ratio was determined using the following formula:

$$\text{Swelling ratio } (\%) = \frac{W_t - W_0}{W_0} \times 100 \quad (1)$$

where W_0 represents weight of the hydrogel beads at time 0 min and W_t is the weight of the beads at a given time.

2.8. In vitro release of sCT

The *in vitro* release profile of sCT from different bead types was evaluated by immersing the dried beads in SGF (pH 1.2) for 2.5 h, followed by SIF (pH 6.8) for an additional 4 h, and subsequently in SCF (pH 7.4) for up to 30 h in total. In brief, a defined number of freeze-dried beads was placed in vials containing 10 mL SGF and incubated at 37 °C for 2.5 h. Following this, the SGF was completely removed and substituted with an equal volume of SIF, and the beads were incubated for an additional 4 h. Finally, the release medium was totally replaced with SCF, and incubation continued until a total time reached 30 h. During the release study, 3 mL of release medium was withdrawn at predetermined time and replenished with a same volume of fresh medium. The concentration of sCT in the release environment was quantified using the Bradford protein assay, which measures protein concentration based on maximum absorbance at 595 nm. The cumulative release of sCT was calculated using Eq. (2) below:

$$\text{Cumulative release of sCT } (\%) = \frac{V_o C_t + V \sum_{n=1}^{t-1} C}{W} \text{ x } 100 \quad (2)$$

where V_o represents total volume of the release medium (10 mL), V is the volume withdrawn at each predetermined time point (3 mL), C_t denotes the concentration of sCT in the release medium at time t, C is the concentration of sCT at the previous time point t-1, and W corresponds to weight of sCT in the tested beads.

2.9. Bioadhesion study

For the bioadhesion study, a fresh segment of the small intestine was obtained from a male chicken and thoroughly rinsed with saline solution to remove any residues. The intestine was then dissected lengthwise, laid flat, and mounted onto a glass support for the experiment. To evaluate the adhesive property, the freeze-dried beads were first soaked in SGF at 37 °C for 2.5 h before being applied to the intestinal tissues. The tissues were subsequently underwent consecutive washes with SIF buffer (pH 6.8) for 15 min to mimic dynamic physiological conditions. Throughout the experiment, photographic documentation was utilized to capture and monitor the adhesive behavior of the beads.

2.10. Hemocompatibility assay

For the hemocompatibility test, blood was obtained from the mice using the cardiac puncture technique [35]. Red blood cells (RBCs) were separated by centrifugation at 3000 rpm for 10 min. The collected erythrocytes were washed three times with PBS and were subsequently diluted to a final concentration of 10 % v/v. In a 1.5 mL tube containing 5 mg dry bead powder, 0.9 mL PBS solution was mixed with 0.1 mL of the RBC suspension and incubated at 37 °C for 4 h. Following incubation, the samples were centrifuged again at 3000 rpm for 10 min, and 100 μL of the supernatant was transferred to a 96-well plate for absorbance measurement at 540 nm using a microplate reader (MicroTek). In this experiment, PBS served as the negative control, while 0.1 % Triton X-100 was employed as the positive control. The percentage of hemolysis for each sample was calculated using the following formula [36]:

$$\text{Hemolysis ratio } (\%) = \frac{OD_{sample} - OD_{negative}}{OD_{positive} - OD_{negative}} \times 100 \quad (3)$$

2.11. Chick CAM assay

The biocompatibility of the hydrogel beads was assessed using chicken egg embryos, with the test procedure conducted on the chick CAM [37]. Fertilized eggs were incubated at condition of 37 °C and 60 % moisture. On day 10, a small section of the eggshell was carefully removed to expose the CAM of the embryo. To prevent infection, the freeze-dried beads were UV- sterilized before being carefully placed onto the CAM surface. The eggshells were then sealed with parafilm, and the implanted eggs were returned to the incubator. After 5 and 7 days of treatment, the implantation site was reopened for visual examination of the CAM and the beads. Comprehensive documentation, including photographic records, was collected to evaluate the safety and biocompatibility of the hydrogel beads.

2.12. In vitro cytotoxicity

CT-26 cells were cultivated in DMEM supplemented with 10 % (*v*/v) FBS, 1 % (v/v) penicillin (100 $U{\cdot}mL^{-1}$), and streptomycin (100 $\mu g{\cdot}mL^{-1}$). Incubation was performed in a 37 °C incubator, maintaining a 5 % CO_2 atmosphere and 95 % humidity. Regular subculturing was performed by detaching the cells with trypsin-EDTA (0.25 % *w*/w), and cell density was assessed using a hemocytometer prior to each experiment.

For the *in vitro* cytotoxicity assessment, the 3-(4,5-dimethylthiazol-2-yl)-2,5-diphenyltetrazolium bromide (MTT) assay was employed [38]. Cells were seeded in 96-well plates at a density of 10,000 cells per well and cultured in a 5 % CO_2 atmosphere at 37 °C for 24 h. Subsequently, the cells were exposed to 100 μL serum-free suspensions containing various concentrations (0–1000 $\mu g{\cdot}mL^{-1}$) of CB, PCB, and PCB@MSNs. After 24 h of incubation, the cells underwent a PBS wash and were then incubated with 100 μL of MTT solution (0.5 $mg{\cdot}mL^{-1}$) for 4 h. Finally, the supernatant in each well was replaced with 150 μL of dimethyl sulfoxide and the optical density value of each well at 570 nm was measured using a microplate reader (Molecular Devices, USA). Untreated cells served as negative controls, representing 100 % cell viability.

2.13. In vitro cellular uptake of RhB-sCT

Rhodamine B-labeled sCT (RhB-sCT) was used to visually observe the cellular uptake of sCT. Briefly, a 4.5 mg/mL solution of chitosan in 1 % glacial acetic acid was prepared. Separately, MSNs were dispersed in PBS solution (1 mg/mL), and RhB-sCT was added to achieve a 1:1 (w/w) ratio. The two solutions were then mixed in a 1:1 (v/v) ratio, followed by the addition of pectin at a concentration of 3 mg/mL to prepare the PCB@MSNs-RhB-sCT precursor. The sample without MSNs was labeled as the PCB-RhB-sCT precursor. CT-26 cells were seeded at a density of 1 $\times$ 10^5 cells per well in 6-well plates and incubated for 24 h. The cells were then treated with PCB-RhB-sCT and PCB@MSNs-RhB-sCT precursors at 37 °C for 2 h, followed by PBS washing for fluorescence imaging. The fluorescence intensity of RhB was adjusted to ensure uniform RhB concentration. After the incubation, the cells were stained with MitoTracker Green and Hoechst dye at room temperature and imaged using a Nikon A1R confocal microscope.

2.14. Statistical analysis

A two-tailed Student's *t*-test was used for comparisons between groups, while one-way ANOVA was used for multiple comparisons. A significance level of $p < 0.05$, calculated using GraphPad Prism 10.4.0, was considered indicative of a statistically significant difference.

3. Results and discussion

3.1. Synthesis and characterization of MSNs

The Fe_3O_4 NPs were successfully synthesized *via* the co-precipitation method. After drying, the Fe_3O_4 NPs appeared as a black powder, as illustrated in the inset of Fig. 2A. SEM and TEM analyses (Fig. 2A) revealed that the Fe_3O_4 NPs possessed a spherical morphology with an average diameter ranging from 15 to 20 nm. The particles were observed to aggregate into larger clusters, likely due to the magnetic interactions inherent to the material.

MSNs were inherently exhibited in the form of a white powder, as

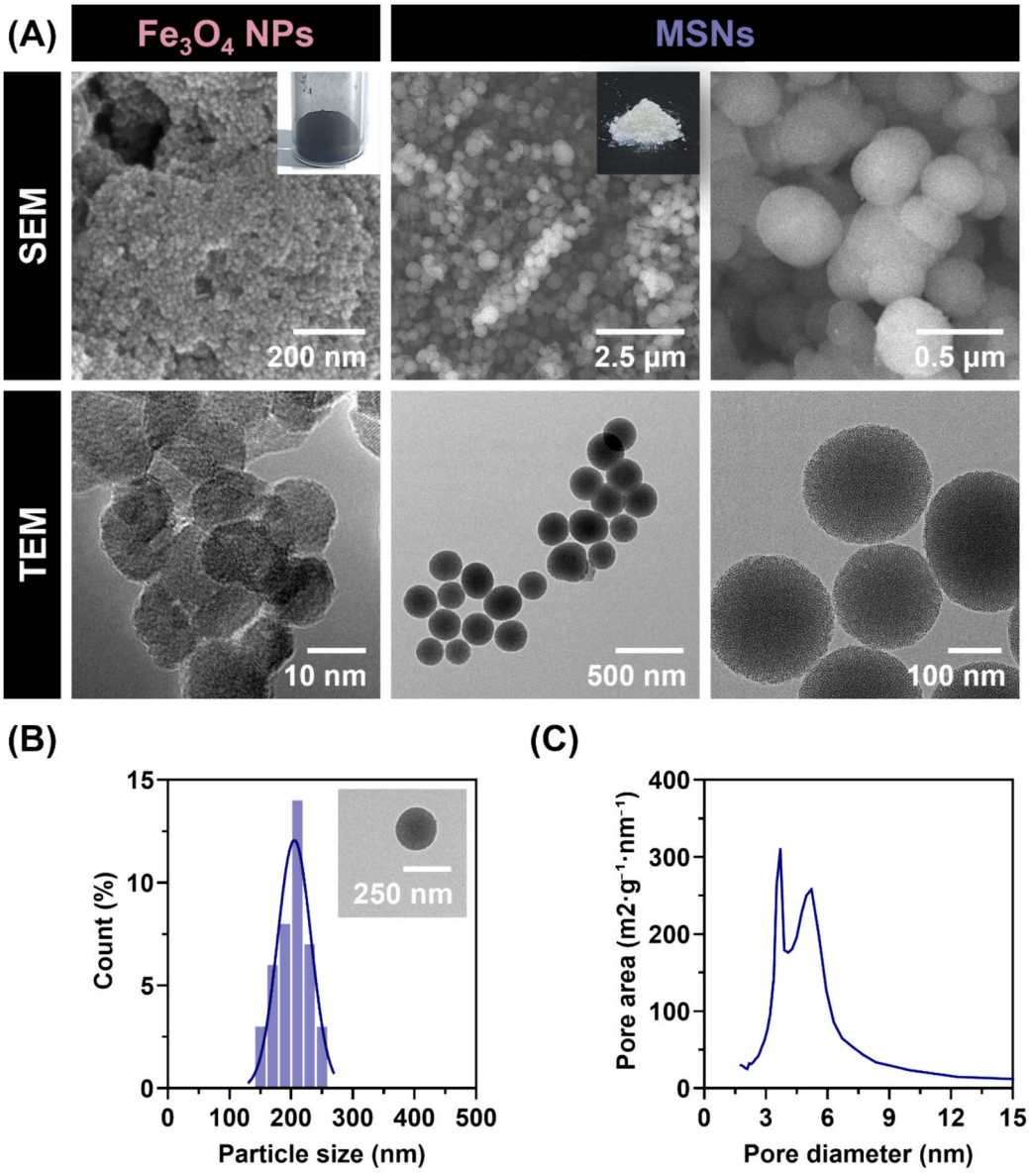

Fig. 2. Synthesis and characterization of MSNs. (A) SEM and TEM images of the Fe_3O_4 NPs and MSNs. The inset photograph shows the dried samples of each type of nanoparticle. (B) Histogram of the particle size distribution of the MSNs. (C) Pore size distribution of MSNs determined by BET method.

depicted in the inset of Fig. 2A. SEM analysis showed that the nanoparticles appeared predominantly spherical with a uniform distribution. TEM imaging further confirmed the presence of a well-defined porous structure. In the synthesis process, both Fe_3O_4 NPs and CTAB were utilized as temporary frameworks and subsequently removed to generate the porous structure. Based on TEM images, the absence of black dots strongly confirmed the complete elimination of Fe_3O_4 NPs. This outcome validates the successful synthesis of mesoporous silica nanoparticles. The particle size distribution of the MSNs, measured manually using ImageJ software, is shown in Fig. 2B, with an average size of 205.1 ± 27.1 nm.

The successful creation of mesoporous structures in silica nanoparticles leads to a substantially increased surface area, thereby significantly enhancing their drug-loading capacity. Consequently, the specific surface area of the synthesized MSNs was evaluated using the BET model for low-temperature N_2 adsorption, while the pore size and

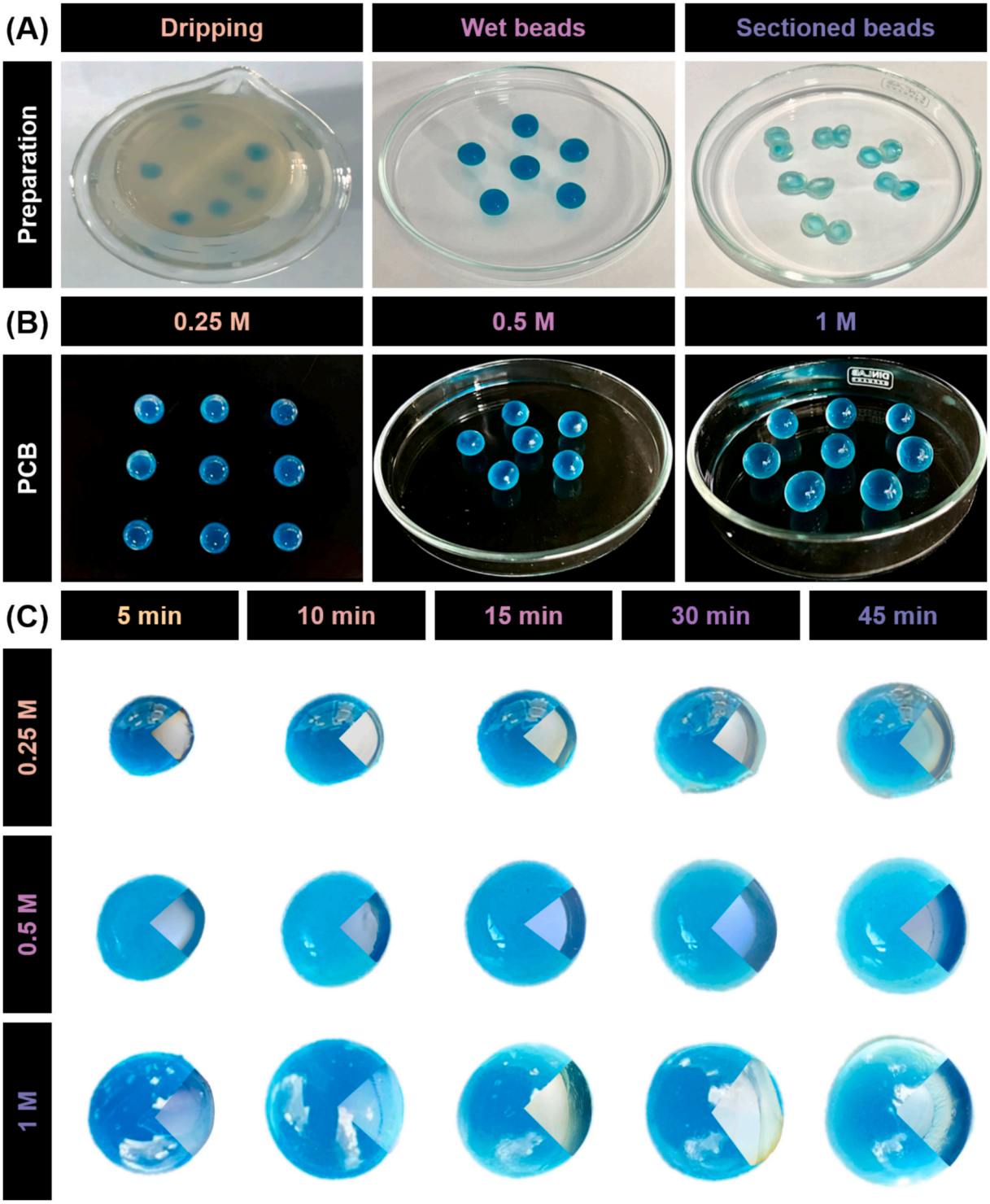

Fig. 3. Synthesis of hydrogel beads. (A) Preparation procedure of core-shell hydrogel beads. (B) Optical images of the hydrogel beads prepared with different concentrations of Ca^{2+} ions. (C) The effect of incubation time in pectin solution and Ca^{2+} concentration on the size of hydrogel beads was demonstrated through optical images, with inset visuals illustrating the cross-sectional conical view of shell thickness recorded using a microscope.

volume were determined through Barrett–Joyner–Halenda analysis [39]. Fig. 2C illustrates the material's pore characteristics. The results revealed pore diameters ranging from 3 to 6 nm, making the MSNs highly suitable for peptide loading.

3.2. Synthesis of core-shell hydrogel beads

Pectin-chitosan core-shell hydrogel beads were synthesized using a straightforward one-pot gelation method that did not require the use of toxic chemical cross-linkers. It is well-established that pectin undergoes gelation upon the introduction of $CaCl_2$ [40]. The addition of divalent cations such as Ca^{2+}, Zn^{2+} interacts with the carboxylic acid groups in the galacturonic acid units of pectin, forming a characteristic "egg-box" structure that results in stable gels [41]. Besides, chitosan, composed of repeating glucosamine units, undergoes a sol-to-gel phase transition when the pH exceeds its pKa (6.3). Chitosan gelation can also occur through hydrogen bonding and hydrophobic interactions [42]. When spherical droplets of chitosan were introduced into a pectin solution, the diffusion of Ca^{2+} and OH^- ions trigger the formation of interlinked gel networks for both pectin and chitosan, ultimately leading to the development of core-shell hydrogel beads.

Fig. 3A illustrates the preparation process for chitosan-pectin beads. The controlled synthesis technique produced uniform spherical beads with clearly defined core-shell structures. The cores of the beads appeared semi-transparent, while the shells exhibited greater transparency. Notably, the beads displayed a distinct border between the core and shell. The mean core diameter could be adjusted by varying the droplet volume, whereas the shell thickness was modulated by altering the $CaCl_2$ concentration (0.25, 0.5, and 1 mol·L^{-1}) and incubation time (5, 10, 15, 30, and 45 min), as shown in Fig. 3B and Fig. 3C.

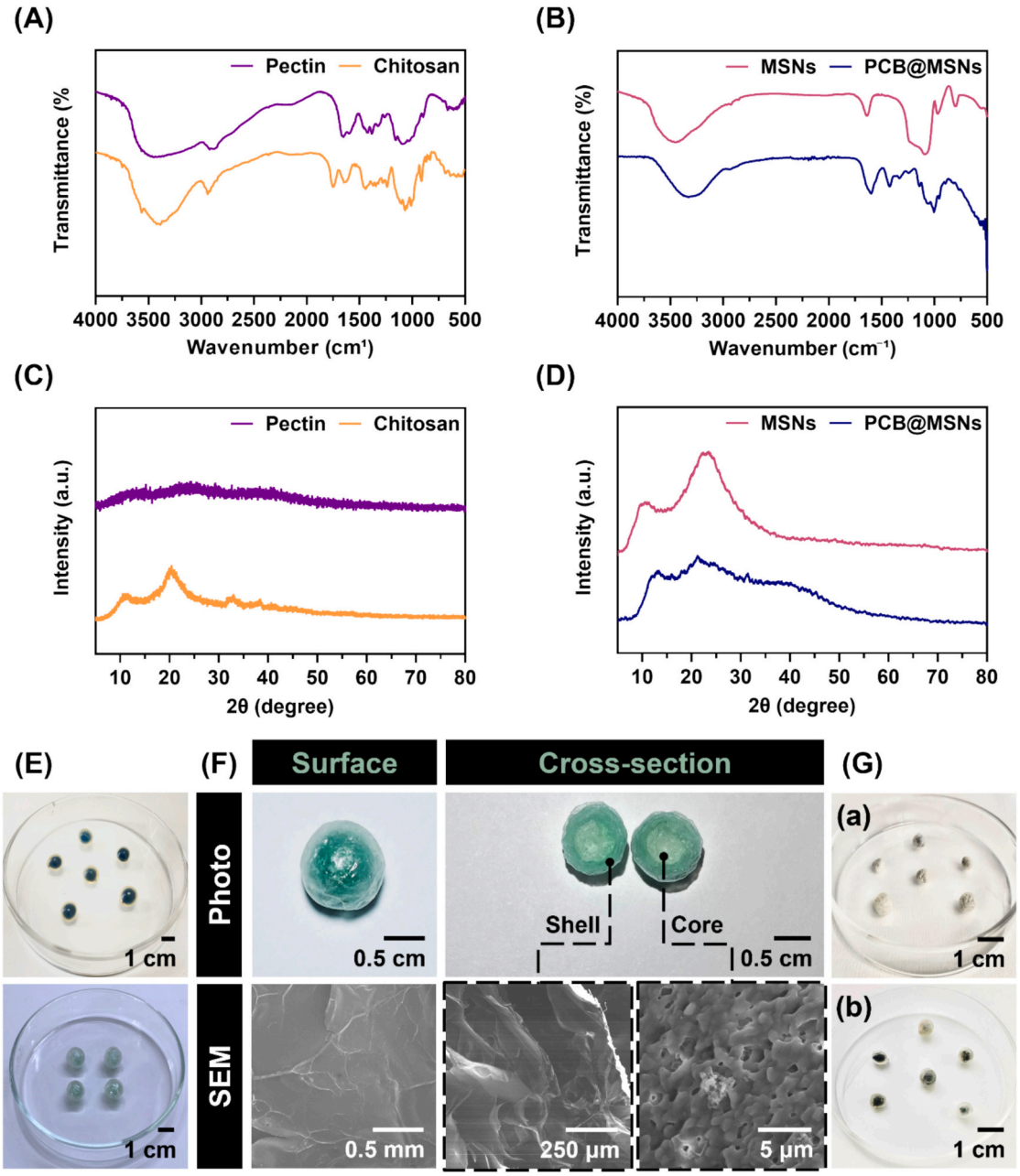

Fig. 4. Characterization of core-shell beads. (A and B) FT-IR spectra of pectin, chitosan, MSNs, and PCB@MSNs. (C and D) XRD spectra of chitosan and pectin beads, MSNs and PCB@MSNs. (E) Optical images of the PCB@MSNs before and after lyophilization. (F) Surface and cross-sectional images at macroscopic and microscopic scale of PCB@MSNs. (G) Preservation of PCB@MSNs by (a) lyophilization and its recovery when (b) soaked in water.

Optical microscopy images of the conical cross-sections provided measurements of the shell thickness, demonstrating the influence of the Ca^{2+} concentration and immersion time. The results showed that increasing either the concentration of Ca^{2+} or the incubation time significantly enhanced the shell thickness and the overall biocapsule volume. Remarkably, the core structure maintained a relatively constant volume, whereas the shell exhibited noticeable thickening. This phenomenon can be attributed to the synthesis process, in which chitosan droplets were introduced into the pectin solution. The chitosan gelled immediately due to the high pH of the pectin solution, resulting in a fixed core volume. In contrast, the pectin shell gelled *via* the egg-box crosslinking mechanism, primarily driven by the diffusion of Ca^{2+} ions from the chitosan core into the surrounding pectin layer. Consequently, higher Ca^{2+} concentrations or longer incubation times led to greater crosslinker diffusion, resulting in a thicker shell.

3.3. Characterization of core-shell beads

The chemical structure of the core-shell beads was analyzed using FTIR spectroscopy, as illustrated in Fig. 4A and Fig. 4B. Pristine chitosan and pectin exhibited broad absorption bands at 3500 cm^{-1}, corresponding to O—H and N—H stretching vibrations [43–45]. For MSNs, a prominent peak was observed at 1075 cm^{-1}, attributed to the asymmetric stretching vibrations of Si–O–Si bonds [46], along with a significant peak at 970 cm^{-1} related to Si–OH bending vibrations [47]. As anticipated, the FTIR spectrum of PCB@MSNs core-shell beads displayed all the characteristic peaks of pectin, chitosan, and MSNs. Notably, the embedding of MSNs within the beads caused a shift in the asymmetric stretching vibration of Si–O–Si bonds to 1034 cm^{-1}, indicating their integration into the core *via* non-covalent interactions with chitosan. Additionally, the O—H and N—H stretching bands of pectin and chitosan shifted to lower wavenumbers, further supporting the formation of the beads through a combination of ionic crosslinking and various physical interactions. These spectral changes confirm the successful incorporation of MSNs into the core-shell structure and the interaction dynamics of the composite materials.

X-ray diffraction (XRD) analysis was employed to examine the amorphous and crystalline characteristics of the pectin and chitosan beads, MSNs, and PCB@MSNs. As shown in Fig. 4C, the absence of diffraction peaks in the pectin pattern confirmed its amorphous nature, whereas small peaks were observed in case of chitosan, indicating its semi-crystalline structure. In Fig. 4D, broad peaks at 10.5° and 23° confirmed the amorphous structure of MSNs. The XRD pattern of PCB@MSNs retained these features of pristine MSNs, pectin and chitosan. Additionally, the XRD results provide an explanation for the differing transparency observed between the core and the shell regions, as noted in Fig. 3.

3.4. Morphology of core-shell beads

As depicted in Fig. 4E, the beads retained their spherical shape and structural uniformity after the freeze-drying process. Notably, the structural integrity of the beads remained intact, underscoring their stability. Following freeze-drying, the beads were sectioned, revealing a compact porous architecture ideal for drug retention and facilitating controlled drug release. These observations highlight the suitability of the core-shell design for its intended applications in drug delivery.

The sectioned bead samples were observed using SEM to evaluate the surface morphology and porous structure of the core-shell beads. As shown in Fig. 4F, the PCB@MSNs displayed a compact surface topography with slight wrinkles, which is favorable for preventing drug leakage and minimizing burst release. Upon magnification, the cross-section of pectin shell revealed a porous structure, which is common characteristic of hydrogel materials. In contrast, the core cross-section exhibited a denser, finer porous structure, with clusters of MSNs embedded within the matrix. This morphology suggests an enhanced capacity for drug loading, reduced leakage, and a controlled release mechanism facilitated by the core's properties.

The stability and reversibility of the core-shell beads were assessed by incubating the dried beads in PBS. As depicted in Fig. 4G, the beads retained their structural integrity and spherical form, preserving their original characteristics. These findings indicate that the prepared beads can be freeze-dried for long-term storage and transportation, while being easily rehydrated for use. This versatility enhances the applicability of the core-shell beads for various drug delivery applications.

3.5. Stability of core-shell hydrogel beads in stimulated fluids

For oral delivery of biodrugs such as proteins and peptides, optimizing drug delivery system requires protecting the therapeutic agent as it passes through the highly acidic environment of the stomach while extending its retention and controlled release in the small intestine to enhance absorption efficiency [48,49]. To demonstrate this, simulated buffer solutions with pH levels representative of key regions of the gastrointestinal tract were used to evaluate the stability and degradation of hydrogel beads, enabling the selection of an optimal crosslinker concentration. The stability of hydrogel beads under these simulated conditions was assessed over a consistent timeframe, as illustrated in Fig. 5A. In gastric fluid at pH 1.2, CB showed signs of disintegration, eventually dissolving completely in the test tube. This outcome indicated that CB alone lacks sufficient stability to survive the stomach environment and reach the small intestine for effective drug release. In contrast, the core-shell bead with an outer pectin shell demonstrated remarkable stability in SGF throughout the evaluation period, showing no signs of disintegration. As the pH increased, the swelling of the pectin shells in SIF and SCF became more pronounced, regardless of the Ca^{2+} concentration used for crosslinking. Among these, PCB_1 exhibited significant disintegration and lost its structural integrity at pH 6.8 and 7.4, whereas PCB_2, PCB_3, and particularly PCB@MSNs largely retained their original morphology under all conditions. These findings highlight the efficacy of the core-shell structure in protecting the biodrug during gastric transit while preserving the structural integrity required for controlled drug release in the intestine.

To further visually compare the stability of CB and PCB@MSNs under SGF condition, the beads were incubated in SGF buffer for an extended period, as shown in Fig. 5B [50]. Consistent with previous observations, CB bead, without the protective pectin shell, began disintegrating within 30 min and completely dissolved in <90 min. In contrast, the PCB@MSNs showed only a slight reduction in size after 90 min, maintaining their structural integrity.

The mucoadhesion capability of hydrogel beads to the intestinal mucous membrane plays a critical role in controlling biodrug delivery [51]. Effective adhesion ensures prolonged retention in the small intestine, allowing the drug to remain in this region for an extended duration and thereby facilitating near-complete release within the targeted area. To simulate these conditions, a chicken small intestine was mounted on a microscope slide at a 30° inclination. The freeze-dried PCBs were pre-soaked in SGF buffer (pH 1.2) for 2.5 h, then applied to the intestinal wall, followed by continuous washing with SIF buffer (pH 6.8) at a flow rate of 50 $mL{\cdot}min^{-1}$ for 15 min to evaluate adhesion performance [49]. As depicted in Fig. 5C, the hydrogel beads maintained strong adhesion to the intestinal wall even after prolonged washing. This mucoadhesive property, combined with the protective capacity and controlled drug release, ensures effective drug absorption in the small intestine, maximizing therapeutic efficacy for the intended treatment.

3.6. Swelling ratio of core-shell beads

The swelling property is a critical factor to evaluate when examining the characteristics of hydrogels [52]. In biological applications, swelling behavior is particularly important as it influences diffusion, mobility,

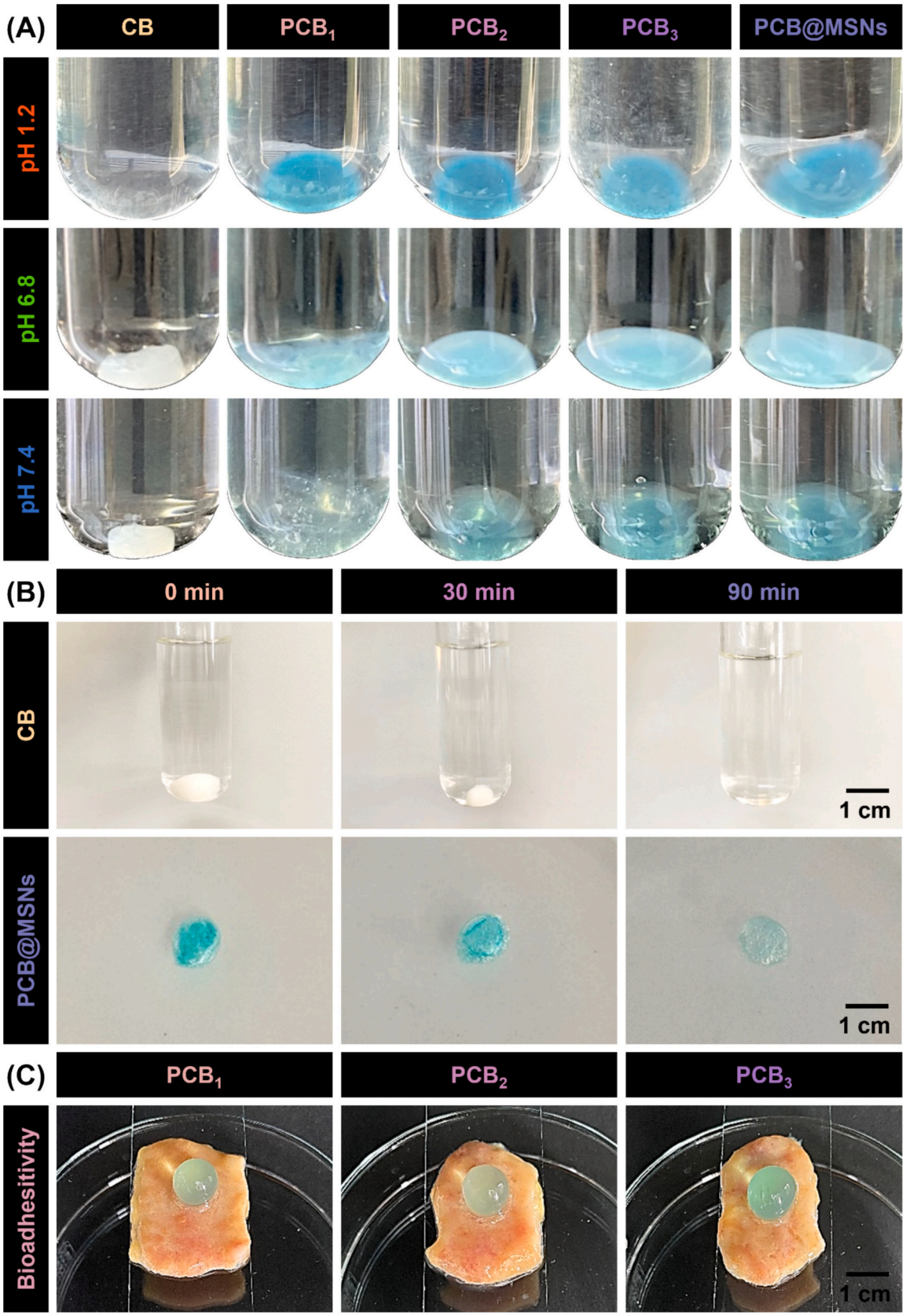

Fig. 5. Stability of beads under simulated fluid conditions. (A) Stability evaluation of hydrogel beads in SGF (pH 1.2), SIF (pH 6.8), and SCF (pH 7.4). (B) Stability assessment of CB and PCB@MSNs in SGF over varying time intervals. (C) Bioadhesive property of hydrogel beads with different Ca^{2+} concentrations on the mucous layer of chicken intestine, subjected to firm washing for 15 min (flow rate: 50 mL·min^{-1}), followed by imaging.

and surface characteristics. Generally, the swelling properties of hydrogel beads are significantly affected by the medium, cross-linking density, and porosity of the hydrogel network. As a polyelectrolyte, pectin exhibits pH-dependent swelling due to the presence of negatively charged carboxylic acid functional groups in its polymer backbone [53]. When immersed in a neutral or alkaline solution, these carboxylic acid groups are converted into negatively charged carboxylate ions, creating electrostatic repulsion between polymer chains [54]. This electrostatic interaction causes the polymer network to swell. In oral drug delivery systems, this pH-responsive swelling plays a vital role in modulating the release of drug molecules, adapting the delivery process to specific gastrointestinal conditions.

The swelling behavior of core-shell hydrogel beads synthesized with varying concentrations of Ca^{2+} cross-linkers (0.25, 0.5, and 1 mol·L^{-1}) was examined in different media at pH 1.2, 6.8, and 7.4. All hydrogel beads exhibited significant swelling property, regardless of the calcium ion concentration and immersion environment, as shown in Fig. 6A–6C. Generally, the swelling ratio decreased as the concentration of Ca^{2+} ions increased, which can be attributed to the higher cross-linking density within the hydrogel network. Additionally, the incorporation of MSNs significantly influenced the swelling ratio. For instance, the swelling ratios of PCB_2 were recorded as 450 %, 1270 %, and 1240 % at pH 1.2, 6.8, and 7.4, respectively. In contrast, PCB@MSNs demonstrated lower swelling ratios of 400 %, 870 %, and 840 % under the same conditions. These findings indicate that the swelling rate of hydrogel beads can be effectively modulated by altering the Ca^{2+} concentration and incorporating MSNs, providing a flexible approach to tailoring hydrogel properties for specific applications.

3.7. *In vitro* sCT release from hydrogel beads in simulated GIT

The release profile of sCT from the hydrogel beads was investigated

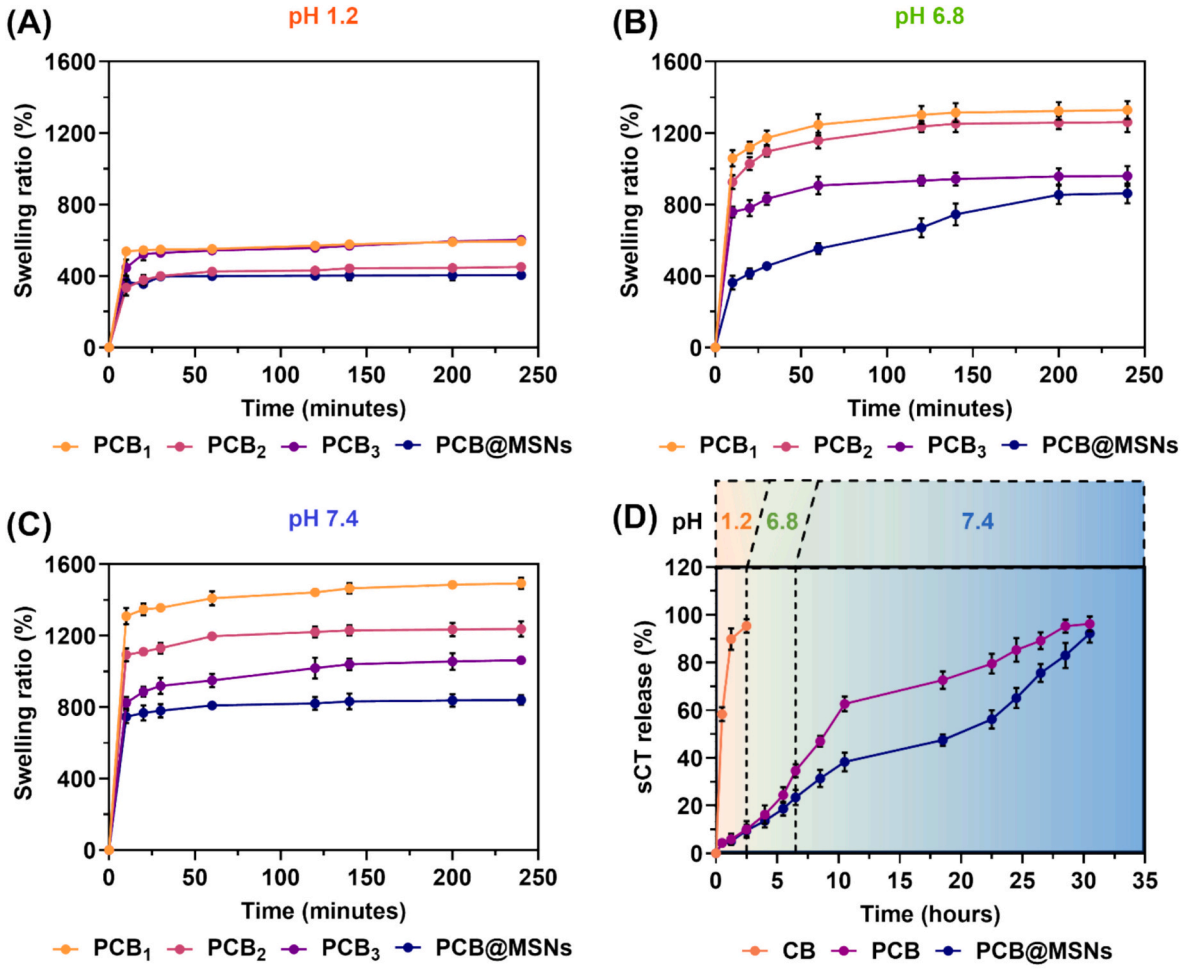

(E)

Fitting models	PCB		PCB@MSNs	
	Regression equations	R^2	Regression equations	R^2
Zero-order	$Q = 0.0293\ t + 0.1342$	0.9356	$Q = 0.0265\ t + 0.0452$	0.9729
First-order	$\log Q = 0.0278\ t - 0.7525$	0.7800	$\log Q = 0.0294\ t - 0.8924$	0.9084
Higuchi	$Q = 21.9023\ t^{1/2} - 22.0757$	0.9736	$Q = 19.2796\ t^{1/2} - 25.5116$	0.9542
Hixson–Crowell	$Q^{1/3} = -0.0976\ t + 4.6899$	0.9735	$Q^{1/3} = -0.0726\ t + 4.7673$	0.9013
Korsmeyer–Peppas	$\log Q = 1.2863 \log t - 1.5340$	0.9884	$\log Q = 0.8237 \log t - 1.3261$	0.9727

Fig. 6. Swelling behavior and sustained release of the hydrogel beads. (A-C) The swelling pattern of the beads was evaluated by incubating them in SGF, SIF, and SCF with their respective pH values. (D) *In vitro* release of sCT from hydrogel beads incubated in various simulated environments with time ($n = 3$). (E) Kinetic studies of sCT release profiles of PCB and PCB@MSNs.

under simulated gastrointestinal conditions. The beads were first incubated in SGF medium (pH 1.2) for 2.5 h, followed by SIF medium (pH 6.8) for 4 h, and finally in colonic medium (pH 7.4) for a total duration of 30 h. As illustrated in Fig. 6D, the release kinetics demonstrated a time- and hydrogel bead-dependent controlled release of sCT. In hydrogel beads lacking a core-shell structure, CB released nearly 95.3 ± 2.8 % of sCT within the first 2.5 h at pH 1.2, indicating the unsuitability of CB as an oral drug carrier. In contrast, the core-shell hydrogel beads exhibited a sustained release profile, suggesting that drug diffusion was maximized in the small intestine region. Notably, the hydrogel bead system containing MSNs released only 31.4 ± 3.6 % of sCT during the initial 8.5 h, highlighting the significant role of electrostatic interactions between chitosan, MSNs, and calcitonin in supporting well-controlled drug release. This controlled release mechanism is critical, as a burst release of sCT could cause hypocalcemia (serum calcium concentration below 8 mg·dL^{-1}), making a sustained release system particularly suitable for practical applications. Moreover, abrupt sCT release can lead to incomplete absorption [55]. Thus, the core-shell structure not only enables controlled drug release but also reduces the loss of sCT in the digestive environment. As expected, PCBs without MSNs showed slightly higher sCT release compared to PCB@MSNs, further demonstrating the influence of MSNs on the controlled release performance.

To gain deeper insights into the drug release mechanism of the system, the release curves of sCT from PCB and PCB@MSNs were fitted to various kinetics models, including zero-order kinetics model, the first-order kinetics model, the Higuchi model, the Hixson-Crowell model, and the Korsmeyer–Peppas model. These models have been widely used to describe drug release behavior from hydrogel matrices [56,57]. The most common mechanism of drug released from hydrogels are diffusion, swelling and erosion. The regression equations along with their R^2 values were presented in the Fig. 6E. Based on the kinetic modeling results, the sCT release from core-shell hydrogel beads most closely aligned with the Korsmeyer-Peppas model. Further analysis of the kinetics within the initial 0–4 h using the Korsmeyer-Peppas equation indicated that the release process during this period was primarily driven by diffusion, attributed to the concentration gradient between the interior and exterior of the beads. In contrast, the subsequent release period was found to depend on the polymer network's expansion, corresponding to the observed disintegration of the hydrogel beads under neutral pH conditions, as demonstrated earlier. Notably, loading sCT into MSNs before incorporation into the chitosan matrix effectively regulated the diffusion-controlled release, extended the release period and reduced the burst release. This result highlights the effectiveness of reinforcing the hydrogel beads with MSNs to achieve a well-regulated and sustained drug delivery system.

3.8. Biocompatibility of hydrogel beads

To evaluate the biocompatibility of the beads at the cellular level, cytotoxicity tests were conducted using CT-26 cells. As shown in Fig. 7A, cell viability remained above 90 %, even at high concentrations of different bead types, including CB, PCB, and PCB@MSNs, after 48 h of co-incubation in a concentration-dependent manner. These results demonstrated excellent biocompatibility, highlighting the potential of these beads as safe and effective carriers for oral therapeutic applications.

The hemocompatibility of the hydrogel beads was further assessed, as depicted in Fig. 7B and Fig. 7C. Triton X-100 and PBS solution were employed as positive and negative controls, with hemolysis levels defined as 100 % and 0 %, respectively. The supernatants of both PCB and PCB@MSNs appeared clear and transparent, comparable to the negative control group. Quantitative analysis indicated that the hemolysis ratio of the beads was consistently below 5 %, demonstrating their excellent hemocompatibility. Additionally, the hemolysis photographs and optical imaging results aligned with the quantitative data, reinforcing these findings. Furthermore, microscopic observations of whole blood cells after incubation with hydrogel beads revealed intact blood cells, further validating the safety of the hydrogel beads for biomedical applications.

3.9. In ovo CAM assay

Biomaterials intended for human applications must exhibit a high degree of biocompatibility [58] In this study, fertilized eggs at embryonic day 10 were utilized to evaluate the biocompatibility of the hydrogel beads. The beads were implanted onto the CAM and incubated at 37 °C for one week, and the development of the chick embryo carefully monitored (Fig. 7F). At day 15, the embryo was observed to be in the appropriate developmental stage, demonstrating survival without any signs of infection. By day 17, the embryo and blood vessels developed normally, further confirming the absence of abnormalities in the embryo. These results provide strong evidence supporting the biocompatibility of the hydrogel beads for potential biomedical applications.

3.10. In vitro cellular uptake of RhB-sCT

The cellular uptake of RhB-sCT-loaded bead precursors was assessed *in vitro* using CT-26 cells, as illustrated in Fig. 7D and Fig. 7E. Among the tested samples, PCB precursor exhibited the highest level of cellular internalization, followed by PCB@MSNs precursor, as confirmed through confocal laser scanning microscopy. This enhanced internalization by CT-26 cells was attributed to the strong electrostatic interactions between the positively charged chitosan units in the bead core and the negatively charged cell membranes.

Moreover, the chitosan components not only facilitated cellular uptake but also improved the beads' permeability through the mucus layer. Interestingly, the mean fluorescence intensity (MFI) of PCB was higher compared to PCB@MSNs, which can be attributed to the controlled release properties imparted by MSN-reinforced beads. These findings underscore the influence of bead composition on cellular uptake and drug release kinetics.

4. Conclusions

This study demonstrates the successful development of MSN-reinforced core-shell hydrogel beads for oral biodrug delivery. The hydrogel beads exhibited excellent biocompatibility, protected the encapsulated biodrug from the harsh gastric environment, and enabled sustained release under intestinal conditions. The innovative core-shell design consisted of a chitosan core embedding sCT- loaded MSNs, ensuring effective drug encapsulation, while the pectin shell allowed tunable shell thickness by adjusting Ca^{2+} concentrations and incubation time, enabling the modulation of bead properties. The system was shown to be stable across the digestive tract, particularly under the challenging gastrointestinal environment. Notably, sCT-loaded core-shell beads exhibited controlled release specifically in the small intestine, optimizing drug bioavailability. Furthermore, the core-shell beads demonstrated high biocompatibility and hemocompatibility, with *in ovo* compatibility test confirming no adverse effects on embryonic development. This study highlights the potential of this system to replace calcitonin injections in the treatment of osteoporosis, offering pain-free administration, improved patient compliance, and fewer side effects. The simplicity, accessibility, and versatility of this platform make it a promising carrier for pharmaceutical applications. In summary, the results indicate that the core-shell hydrogel beads are effective biomaterials for oral biodrug delivery, with potential applications ranging from bone reconstruction to inflammatory disease treatment.

CRediT authorship contribution statement

V.H. Giang Phan: Investigation, Writing – review & editing, Writing – original draft. **Bich-Phuong Thi Nguyen:** Investigation, Writing –

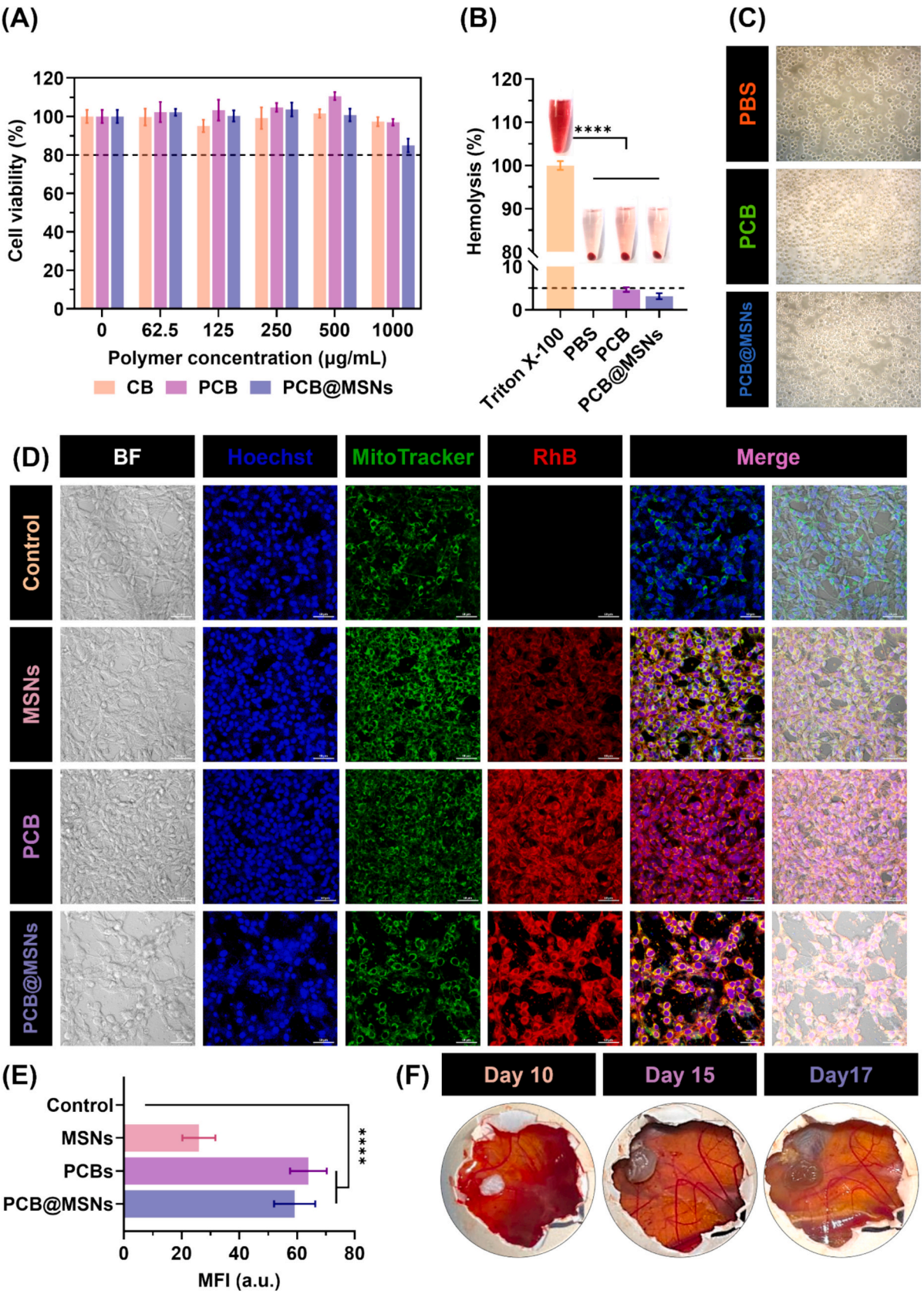

Fig. 7. *In vitro* biocompatibility of hydrogel beads. (A) *In vitro* cell viability of CT-26 cells co-cultured with various concentrations of beads for 48 h ($n = 6$). (B) Hemolysis ratio and inset showing corresponding photographs of hydrogel beads after treatment, with Triton X-100 and PBS used as positive and negative controls, respectively. (C) Images of whole blood cells after treatment with hydrogel beads. (D) Cellular internalization and (E) Fluorescence intensity of RhB-sCT in CT-26 cells. (F) *In ovo* safety assessment of hydrogel beads implanted on the CAM of fertilized eggs.

review & editing, Writing – original draft. **Nhi Yen Nguyen:** Investigation, Writing – review & editing, Writing – original draft. **Cam-Nhung Dinh Tran:** Investigation, Writing – review & editing, Writing – original draft. **Quynh-Nhu Doan Nguyen:** Investigation, Writing – review & editing, Writing – original draft. **Cuong Hung Luu:** Investigation, Writing – review & editing, Writing – original draft. **Panchanathan Manivasagan:** Investigation, Writing – review & editing, Writing – original draft. **Eue-Soon Jang:** Methodology, Writing – review & editing, Writing – original draft. **Deok Chun Yang:** Investigation, Writing – review & editing, Writing – original draft. **Dong Uk Yang:** Investigation, Writing – review & editing, Writing – original draft. **Yi Li:** Validation, Supervision, Conceptualization, Writing – review & editing, Writing – original draft. **João Conde:** Validation, Writing – review & editing, Writing – original draft. **Thavasyappan Thambi:** Validation, Supervision, Data curation, Conceptualization, Writing – review & editing, Writing – original draft.

Declaration of competing interest

J.C. is a co-founder and shareholder of TargTex S.A. – Targeted therapeutics for Glioblastoma Multiforme. J.C. is also a member of the Global Burden Disease (GBD) consortium of the Institute for Health Metrics and Evaluation (IHME), University of Washington (US). All other authors declare no conflicts of interest.

Acknowledgement

This work was supported by Ton Duc Thang University. This work was also supported by the National Research Foundation of Korea (NRF) grant funded by the Korean government (MSIT) (NRF-2023R1A2C1005904). E.-S.J. is incredibly grateful for the research grant from the Korean Ministry of Education, Science & Technology (2016R1D1A3B0201175615), the Korean Health Technology R&D Project (HP23C0260) through the Korean Health Industry Development Institute (KHIDI) funded by the Ministry of Health and Welfare, and the Innovative Human Resource Development for Local Intellectualization Support Program (IITP-2025-RS-2020-II201612) through the Institute of Information & Communications Technology Planning & Evaluation (IITP) funded by the Korean government (MSIT), Republic of Korea. The Basic Science Research Program supported this research through the National Research Foundation of Korea (NRF), funded by the Ministry of Education (NRF-2022R1I1A1A01068693).

Data availability

The data that support the findings of this study are available from the corresponding author upon reasonable request.

References

[1] S. Mehrotra, P. Kalyan Bg, P.G. Nayak, A. Joseph, J. Manikkath, Recent Progress in the Oral delivery of therapeutic peptides and proteins: overview of pharmaceutical strategies to overcome absorption hurdles, Adv, Pharm. Bull. 14 (1) (2024) 11–33.
[2] A. Deepak, A.K. Goyal, G. Rath, Nanofiber in transmucosal drug delivery, J. Drug Deliv. Sci. Technol. 43 (2018) 379–387.
[3] J.K.W. Lam, C.C.K. Cheung, M.Y.T. Chow, E. Harrop, S. Lapwood, S.I.G. Barclay, I. C.K. Wong, Transmucosal drug administration as an alternative route in palliative and end-of-life care during the COVID-19 pandemic, Adv. Drug Deliv. Rev. 160 (2020) 234–243.
[4] Q. Zhu, Z. Chen, P.K. Paul, Y. Lu, W. Wu, J. Qi, Oral delivery of proteins and peptides: challenges, status quo and future perspectives, Acta Pharm. Sin. B 11 (8) (2021) 2416–2448.
[5] J. Lou, H. Duan, Q. Qin, Z. Teng, F. Gan, X. Zhou, X. Zhou, Advances in Oral drug delivery systems: challenges and opportunities, Pharmaceutics 15 (2) (2023).
[6] A. Rivera del Rio, J.K. Keppler, R.M. Boom, A.E.M. Janssen, Protein acidification and hydrolysis by pepsin ensure efficient trypsin-catalyzed hydrolysis, Food Funct. 12 (10) (2021) 4570–4581.
[7] D.J.L. Mat, T. Cattenoz, I. Souchon, C. Michon, S. Le Feunteun, Monitoring protein hydrolysis by pepsin using pH-stat: in vitro gastric digestions in static and dynamic pH conditions, Food Chem. 239 (2018) 268–275.
[8] A. Ren, J. Hu, C. Qin, N. Xia, M. Yu, X. Xu, H. Yang, M. Han, L. Zhang, L. Ma, Oral administration microrobots for drug delivery, Bioact. Mater. 39 (2024) 163–190.
[9] M.S. Alqahtani, M. Kazi, M.A. Alsenaidy, M.Z. Ahmad, Advances in Oral drug delivery, Front. Pharmacol. 12 (2021) 618411.
[10] B. Liang, G. Burley, S. Lin, Y.-C. Shi, Osteoporosis pathogenesis and treatment: existing and emerging avenues, Cell. Mol. Biol. Lett. 27 (1) (2022) 72.
[11] J. Xie, J. Guo, Z. Kanwal, M. Wu, X. Lv, N.A. Ibrahim, P. Li, M.A. Buabeid, E. A. Arafa, Q. Sun, Calcitonin and bone physiology, In Vitro, In Vivo, and Clinical Investigations, Int. J. Endocrinol. 2020 (2020) 3236828.
[12] S. Ahmadipour, J. Varshosaz, B. Hashemibeni, L. Safaeian, M. Manshaei, A. Sarmadi, Calcitonin-loaded octamaleimic acid-silsesquioxane nanoparticles in hydrogel scaffold support osteoinductivity in bone regeneration, Pharm. Dev. Technol. 26 (2) (2021) 220–232.
[13] P. Yu, Y. Chen, Y. Wang, Y. Liu, P. Zhang, Q. Guo, S. Li, H. Xiao, J. Xie, H. Tan, J. Li, Pentapeptide-decorated silica nanoparticles loading salmon calcitonin for in vivo osteoporosis treatment with sustained hypocalcemic effect, Mater. Today Chem. 14 (2019) 100189.
[14] C.-Y. Hsiao, T.-H. Chen, T.-H. Chu, Y.-N. Ting, P.-J. Tsai, J.-F. Shyu, Calcitonin induces bone formation by increasing expression of Wnt10b in osteoclasts in Ovariectomy-induced osteoporotic rats, Front. Endocrinol. 11 (2020).
[15] M.A. Karsdal, I. Byrjalsen, K. Henriksen, B.J. Riis, C. Christiansen, A pharmacokinetic and Pharmacodynamic comparison of synthetic and recombinant Oral Salmon calcitonin, J. Clin. Pharmacol. 49 (2) (2009) 229–234.
[16] S. Lee, Development of high affinity calcitonin analog fragments targeting extracellular domains of calcitonin family receptors, Biomolecules 11 (9) (2021) 1364.
[17] D. Luo, X. Ni, H. Yang, L. Feng, Z. Chen, L. Bai, A comprehensive review of advanced nasal delivery: specially insulin and calcitonin, Eur. J. Pharm. Sci. 192 (2024) 106630.
[18] R.B. Shah, M.A. Khan, Protection of salmon calcitonin breakdown with serine proteases by various ovomucoid species for oral drug delivery, J. Pharm. Sci. 93 (2) (2004) 392–406.
[19] M. Vertzoni, P. Augustijns, M. Grimm, M. Koziolek, G. Lemmens, N. Parrott, C. Pentafragka, C. Reppas, J. Rubbens, J. Van Den Abeele, T. Vanuytsel, W. Weitschies, C.G. Wilson, Impact of regional differences along the gastrointestinal tract of healthy adults on oral drug absorption: an UNGAP review, Eur. J. Pharm. Sci. 134 (2019) 153–175.
[20] S. Hua, Advances in Oral drug delivery for regional targeting in the gastrointestinal tract - influence of physiological, Pathophysiological and Pharmaceutical Factors, Front. Pharmacol. 11 (2020) 524.
[21] R. Yamamura, K.Y. Inoue, K. Nishino, S. Yamasaki, Intestinal and fecal pH in human health, Front. Microb. 2 (2023) 1192316.
[22] M. Azman, A.H. Sabri, Q.K. Anjani, M.F. Mustaffa, K.A. Hamid, Intestinal absorption study: challenges and absorption enhancement strategies in improving Oral drug delivery, Pharmaceuticals (Basel) 15 (8) (2022) 975.
[23] Y.N. Gavhane, A.V. Yadav, Loss of orally administered drugs in GI tract, Saudi Pharm. J. 20 (4) (2012) 331–344.
[24] M.S. Alqahtani, M.S. Islam, S. Podaralla, R.S. Kaushik, J. Reineke, T. Woyengo, O. Perumal, Food Protein Based Core–Shell Nanocarriers for Oral Drug Delivery: Effect of Shell Composition on in Vitro and in Vivo Functional Performance of Zein Nanocarriers, Mol. Pharm. 14 (3) (2017) 757–769.
[25] G.O. Taylan, C. Illanes-Bordomás, O. Guven, E. Erkan, S.Ç. Erünsal, M.H. Oztop, C. A. García-González, Core-shell aerogel design for enhanced oral insulin delivery, Int. J. Pharm. 669 (2025) 125038.
[26] C. Li, L. Yuan, X. Zhang, A. Zhang, Y. Pan, Y. Wang, W. Qu, H. Hao, S.A. Algharib, D. Chen, S. Xie, Core-shell nanosystems designed for effective oral delivery of polypeptide drugs, J. Control. Release 352 (2022) 540–555.
[27] P.-K.T. Ngo, D.N. Nguyen, H.-P. Nguyen, T.-H.H. Tran, Q.-N.D. Nguyen, C.H. Luu, T.-H. Phan, P.K. Le, V.H.G. Phan, H.T. Ta, T. Thambi, Silk fibroin/chitosan/montmorillonite sponge dressing: enhancing hemostasis, antimicrobial activity, and angiogenesis for advanced wound healing applications, Int. J. Biol. Macromol. 279 (2024) 135329.
[28] H. Choukaife, S. Seyam, B. Alallam, A.A. Doolaanea, M. Alfatama, Current advances in chitosan nanoparticles based Oral drug delivery for colorectal Cancer treatment, Int. J. Nanomedicine 17 (2022) 3933–3966.
[29] C.M. Phan, C.H. Luu, M. Murugesan, T.-N.-Q. Nguyen, N.-Y.N. Ha, H.L. Ngo, N.-D. H. Nguyen, Z. Pan, V.H.G. Phan, Y. Li, T. Thambi, Injectable gelatin-pectin hydrogel for dental tissue engineering: enhanced angiogenesis and antibacterial efficacy for pulpitis therapy, Int. J. Biol. Macromol. 284 (2025) 137939.
[30] D. Li, J. Li, H.-L. Dong, X. Li, J.-Q. Zhang, S. Ramaswamy, F. Xu, Pectin in biomedical and drug delivery applications: a review, Int. J. Biol. Macromol. 185 (2021) 49–65.
[31] N. Raghav, C. Vashisth, N. Mor, P. Arya, M.R. Sharma, R. Kaur, S.P. Bhatti, J. F. Kennedy, Recent advances in cellulose, pectin, carrageenan and alginate-based oral drug delivery systems, Int. J. Biol. Macromol. 244 (2023) 125357.
[32] Y. Li, V.H. Giang Phan, Z. Pan, X. Xuan, H.Y. Yang, C.H. Luu, T.-H. Phan, T.M.D. Le, T. Thambi, Integrated and hyaluronic acid-coated mesoporous silica nanoparticles conjugated with cisplatin and chlorin e6 for combined chemo and photodynamic cancer therapy, Eur. Polym. J. 220 (2024) 113426.
[33] H.-C. Luu, C.Q. Ngo, N.H. Nguyen, D.L. Tran, D.H. Nguyen, C.K. Nguyen, Polyamidoamine dendrite-tailored mesoporous nanosilica surfaces for high drug loading and controlled release, Vietnam J. Sci. Technol. Eng. 65 (1) (2023) 25–31.
[34] D. Kwon, B.G. Cha, Y. Cho, J. Min, E.-B. Park, S.-J. Kang, J. Kim, Extra-large pore mesoporous silica nanoparticles for directing in vivo M2 macrophage polarization by delivering IL-4, Nano Lett. 17 (5) (2017) 2747–2756.

[35] C.H. Luu, N.-T. Nguyen, H.T. Ta, Unravelling surface modification strategies for preventing medical device-induced thrombosis, Adv. Healthc. Mater. 13 (1) (2024) 2301039.
[36] T.-H.H. Tran, C.H. Luu, K.-T.T. Nguyen, M.-A.L. Hoang, Q.-K. Pham, C.M. Phan, N.-K.-L. Thai, H.T. Nguyen, T. Thambi, V.H.G. Phan, Mineralized biopolymers-based scaffold encapsulating with dual drugs for alveolar ridge preservation, Macromol. Biosci. 25 (2) (2024) 2400351.
[37] V.H.G. Phan, H.-S. Duong, Q.-G.T. Le, G. Janarthanan, S. Vijayavenkataraman, H.-N.H. Nguyen, B.-P.T. Nguyen, P. Manivasagan, E.-S. Jang, Y. Li, T. Thambi, Nanoengineered injectable hydrogels derived from layered double hydroxides and alginate for sustained release of protein therapeutics in tissue engineering applications, J. Nanobiotechnol. 21 (1) (2023) 405.
[38] C.H. Luu, D.T.D. Nguyen, C.Y. Chee, T.C.N. Thi, D.Y.P. Nguyen, D.H. Nguyen, C. K. Nguyen, Thermal and redox responsive polyamidoamine dendrimer–poly(N-isopropylacrylamide) bridged by disulfide linkages for targeted and controlled drug delivery system, J. Appl. Polym. Sci. 140 (27) (2023) e54108.
[39] N. Joudeh, D. Linke, Nanoparticle classification, physicochemical properties, characterization, and applications: a comprehensive review for biologists, J. Nanobiotechnol. 20 (1) (2022) 262.
[40] Y. Yang, G. Zhang, Y. Hong, Z. Gu, F. Fang, Calcium cation triggers and accelerates the gelation of high methoxy pectin, Food Hydrocoll. 32 (2) (2013) 228–234.
[41] L. Cao, W. Lu, A. Mata, K. Nishinari, Y. Fang, Egg-box model-based gelation of alginate and pectin: a review, Carbohydr. Polym. 242 (2020) 116389.
[42] M. Yadav, B. Kaushik, G.K. Rao, C.M. Srivastava, D. Vaya, Advances and challenges in the use of chitosan and its derivatives in biomedical fields: a review, Carbohyd. Polym. Technol. Appl. 5 (2023) 100323.
[43] D.M. Suflet, I. Popescu, I.M. Pelin, D.L. Ichim, O.M. Daraba, M. Constantin, G. Fundueanu, Dual cross-linked chitosan/PVA hydrogels containing silver nanoparticles with antimicrobial properties, Pharmaceutics 13 (9) (2021) 1461.
[44] S. Lal, V. Kumar, S. Arora, Eco-friendly synthesis of biodegradable and high strength ternary blend films of PVA/starch/pectin: mechanical, thermal and biodegradation studies, Polym. Polym. Compos. 29 (9) (2020) 1505–1514.
[45] V.H. Giang Phan, T.-H. Hoang Tran, T.-K. Ngoc Nguyen, T. Thambi, X. Murgia, D.-K. Ho, D.R. Elmaleh, Triple-hybrid BioScaffold based on silk fibroin, chitosan, and nano-biphasic calcium phosphates: preparation, characterization of physiochemical and biopharmaceutical properties, J. Pharm. Sci. 113 (8) (2024) 2286–2295.
[46] T. Jutarosaga, J.S. Jeoung, S. Seraphin, Infrared spectroscopy of Si–O bonding in low-dose low-energy separation by implanted oxygen materials, Thin Solid Films 476 (2) (2005) 303–311.
[47] A. Presentato, F. Armetta, A. Spinella, D.F. Chillura Martino, R. Alduina, M. L. Saladino, Formulation of mesoporous silica nanoparticles for controlled release of antimicrobials for stone preventive conservation, Frontiers, Chemistry 8 (2020) 699.
[48] Z. Luo, N. Paunović, J.-C. Leroux, Physical methods for enhancing drug absorption from the gastrointestinal tract, Adv. Drug Deliv. Rev. 175 (2021) 113814.
[49] V.H.G. Phan, R. Mathiyalagan, M.-T. Nguyen, T.-T. Tran, M. Murugesan, T.-N. Ho, H. Huong, D.C. Yang, Y. Li, T. Thambi, Ionically cross-linked alginate-chitosan core-shell hydrogel beads for oral delivery of insulin, Int. J. Biol. Macromol. 222 (2022) 262–271.
[50] S. Ahadian, J.A. Finbloom, M. Mofidfar, S.E. Diltemiz, F. Nasrollahi, E. Davoodi, V. Hosseini, I. Mylonaki, S. Sangabathuni, H. Montazerian, K. Fetah, R. Nasiri, M. R. Dokmeci, M.M. Stevens, T.A. Desai, A. Khademhosseini, Micro and nanoscale technologies in oral drug delivery, Adv. Drug Deliv. Rev. 157 (2020) 37–62.
[51] S. Zhang, J. Ermann, M.D. Succi, A. Zhou, M.J. Hamilton, B. Cao, J.R. Korzenik, J. N. Glickman, P.K. Vemula, L.H. Glimcher, G. Traverso, R. Langer, J.M. Karp, An inflammation-targeting hydrogel for local drug delivery in inflammatory bowel disease, Sci. Transl. Med. 7 (300) (2015) 300ra128.
[52] E.M. Ahmed, Hydrogel: preparation, characterization, and applications: a review, J. Adv. Res. 6 (2) (2015) 105–121.
[53] J. Singh, P. Nayak, pH-responsive polymers for drug delivery: trends and opportunities, J. Polym. Sci. 61 (22) (2023) 2828–2850.
[54] B. Kost, M. Basko, M. Bednarek, M. Socka, B. Kopka, G. Łapienis, T. Biela, P. Kubisa, M. Brzeziński, The influence of the functional end groups on the properties of polylactide-based materials, Prog. Polym. Sci. 130 (2022) 101556.
[55] J. Xie, J. Guo, Z. Kanwal, M. Wu, X. Lv, N.A. Ibrahim, P. Li, M.A. Buabeid, E.-S. A. Arafa, Q. Sun, Calcitonin and bone physiology: in vitro, in vivo, and clinical investigations, Int. J. Endocrinol. 2020 (1) (2020) 3236828.
[56] K.M. Sahu, A. Biswal, U. Manisha, S.K. Swain, Synthesis and drug release kinetics of ciprofloxacin from polyacrylamide/dextran/carbon quantum dots (PAM/Dex/CQD) hydrogels, Int. J. Biol. Macromol. 269 (2024) 132132.
[57] Pragnesh N. Dave, Pradip M. Macwan, Bhagvan Kamaliya, Biodegradable gg-cl-poly (NIPAm-co-AA)/—o-MWCNT based hydrogel for combined drug delivery system of metformin and sodium diclofenac: in vitro studies, RSC Adv. 13 (33) (2023) 22875–22885.
[58] P. Trucillo, Biomaterials for drug delivery and human applications, Materials (Basel) 17 (2) (2024) 456.